YALE JOURNAL OF BIOLOGY AND MEDICINE 91 (2018), pp.257-266.

REVIEW

YJBM

Investigation of Endothelial Surface Glycocalyx Components and Ultrastructure by Single Molecule Localization Microscopy: Stochastic Optical Reconstruction Microscopy (STORM)

Yifan Xia and Bingmei M. Fu*

Department of Biomedical Engineering, The City College of the City University of New York, New York, NY

On the luminal surface of our blood vessels, there is a thin layer called endothelial surface glycocalyx (ESG†) which consists of proteoglycans, glycosaminoglycans (GAGs), and glycoproteins. The GAGs in the ESG are heparan sulfate (HS), hyaluronic acid (HA), chondroitin sulfate (CS), and sialic acid (SA). In order to play important roles in regulating vascular functions, such as being a mechanosensor and transducer for the endothelial cells (ECs) to sense the blood flow, a molecular sieve to maintain normal microvessel permeability and a barrier between the circulating cells and endothelial cells forming the vessel wall, the ESG should have an organized structure at the molecular level. Due to the limitations of conventional optical and electrical microscopy, the ultrastructure of ESG, in the order of 10 to 100 nanometers, has not been revealed until recent development of a super resolution fluorescence optical microscope, Stochastic Optical Reconstruction Microscope (STORM), which is one type of single molecule localization microscopy. This short review describes how the STORM can overcome the diffraction barrier in the conventional fluorescence microscopy to identify the chemical components of the ESG at a high spatial resolution. Examples of the organized ultrastructure of the ESG on the *in vitro* EC monolayer revealed by the Nikon-STORM system are given as well as how its components get lost during the onset of sepsis, a systemic inflammatory syndrome induced by bacterial infection, which demonstrate that this new technique can be applied to discover the structural and molecular mechanisms at nanometer scales in the native cellular environment for the cellular functions under normal and disease conditions.

INTRODUCTION

Microscopy plays a crucial role in the biomedical research as it has opened the door of the mini world to us. Due to the Abbe's diffraction limit, *i.e.*, the resolution of a given instrument is proportional to the wavelength of the light being observed, and inversely proportional to the size of its objective, the optical or light microscope has the limited spatial resolution, about several hundred nanometers [1]. Although the electron microscope

*To whom all correspondence should be addressed: Bingmei M. Fu, Department of Biomedical Engineering, The City College of the City University of New York, 160 Convent Ave., New York, NY 10031; Tel: (212)-650-7531, Fax: (212)-650-6727, Email: fu@ccny.cuny.edu.

†Abbreviations: EC, endothelial cell; EM, electron microscopy; ESG, endothelial surface glycocalyx; CS, chondroitin sulfate; GAG, glycosaminoglycan; HA, hyaluronic acid; HS, heparan sulfate; PSF, Point Spread Function; SA, sialic acids; STORM, Stochastic Optical Reconstruction Microscopy; bEnd3, mouse brain microvascular endothelial cell.

Keywords: Endothelial surface glycocalyx, Ultrastructure, STORM, Heparan sulfate, Hyaluronic acid

(EM) and the scanning probe microscope (SPM) have much better spatial resolution, due to artifacts in sample preparations such as dehydration, fixation, and ultrathin cutting, they cannot provide the required spatial-chemical organization and structure information for the biomedical samples.

The luminal surfaces of endothelial cells (ECs) that line our vasculature are coated with a glycocalyx of membrane-bound macromolecules comprised of proteoglycans and glycosaminoglycans (GAGs) [2]. The GAGs in the endothelial surface glycocalyx (ESG) are heparan sulfate (HS), hyaluronic acid (HA), chondroitin sulfate (CS), and sialic acid (SA) [3]. Due to its unique location, at the interface of the circulating blood and the vessel wall, the ESG has been found to play important roles in maintaining normal vascular functions [4]. The roles of the ESG are determined by its composition, structure, and mechanical property, which have been widely studied since the 1960s by a variety of methods. However, due to the limitations of spatial resolutions or artifacts in sample preparations in the previous techniques, the spatio-chemical organization of the ESG remains unclear.

By winning the Nobel prize in Chemistry in 2014, the unique combination of molecule-specific contrast and live-cell imaging capability led fluorescence optical super-resolution microscopy to come back to the center stage of the microscopes, especially for the biomedical samples [5-11]. The recently developed Stochastic Optical Reconstruction Microscopy (STORM), one of three types of single molecule localization microscopy [7], employs organic dyes and fluorescent proteins as photo-switchable emitters to trade temporal resolution for a super spatial resolution (~20 nm lateral and ~50 nm axial at present), which is an order of magnitude higher than conventional confocal microscopy. STORM can perform 2-D [7], 3-D [12], and multicolor [13] imaging. STORM and other types of super resolution optical microscopy enable the discovery and investigation of cellular structures at the nanometer scale, from individual proteins to entire organelles in the native cellular environment [14-16]. This review describes the recent application of STORM to visualize the ESG of cultured ECs under normal and disease conditions.

BEATING THE DIFFRACTION LIMIT OF RESOLUTION BY STORM

Before the super-resolution microscopy was invented, the optical microscope is limited by the diffraction, caused by the wave nature of the lights. This diffraction limit was first discovered by Ernst Abbe in 1873 [1], which indicates that any two spots (emitters) closer than ~ λ/2NA cannot be distinguished from each other. Here λ is the wavelength of the light and NA is the numerical aperture of the objective lens of a microscope. This limit led the development of microscopy to other directions, either decreasing the wavelength out of the range of visible lights, such as electron microscopy, or getting rid of the lights, such as scanning probe microscopy. Due to this diffraction limit of resolution, the development of the optical microscope has been slowed down for decades until recent development of the single- molecule fluorescence technology [17].

The diffraction of a single fluorescence molecule can be described as the point spread function (PSF). When the light of wavelength λ excites the fluorophore (emitter), the intensity profile of the spot is defined as the PSF with the width approximately as 0.6 λ/NA, NA is the numerical aperture of the objective. As a result, two identical emitters separated by a distance less than the width of the PSF would appear as a single object, not distinguished from each other (top plot at the right panel in Figure 1A). The diffraction-limited image resolution, for a high numerical aperture objective lens, is ~250 nm in the lateral direction and ~550 nm in the axial direction, for a conventional fluorescence microscope.

The key idea of the single-molecule localization microscopy is to light the molecule in turn to achieve the nanometer-level accuracy of their position and reconstruction into a super- resolution image, such as Stochastic Optical Reconstruction Microscopy (STORM). Figure 1A demonstrates the working principle of the single-molecule localization microscopy (STORM) by using photo-switching mechanisms to stochastically activate individual molecules (photo-switchable or photoactivatable fluorophores) within the diffraction-limited region at different times. Then images with sub-diffraction limit resolution are reconstructed from the measured positions of individual fluorophores [7]. To localize a molecule, the emitter at that molecule should not have any overlap with its neighbors, so that it can be isolated and fitted into the PSF (middle and bottom plots in Figure 1A). One way to keep the fluorescence molecule emitting in turn is to make the photo-switchable fluorophore blink. To achieve the photo-blinking of the fluorophore is to switch between light and dark states, which are usually called “on” and “off.” “On” is the state in which the fluorophore is able to be excited and its emission can be detected by the camera. The “off” state is in which the fluorophore cannot be excited by the laser, including the temporarily blinking or permanently bleaching. The most important factor for STORM to accomplish sub-diffraction resolution is that the photo-switchable fluorophores are used to maintain neighboring molecules in different states, “on” or “off,” enabling to be distinguished from each other [18].

The number of emitters and the image collecting time are the determinants of the efficiency and accuracy of any microscopy. The higher population of the emitter would

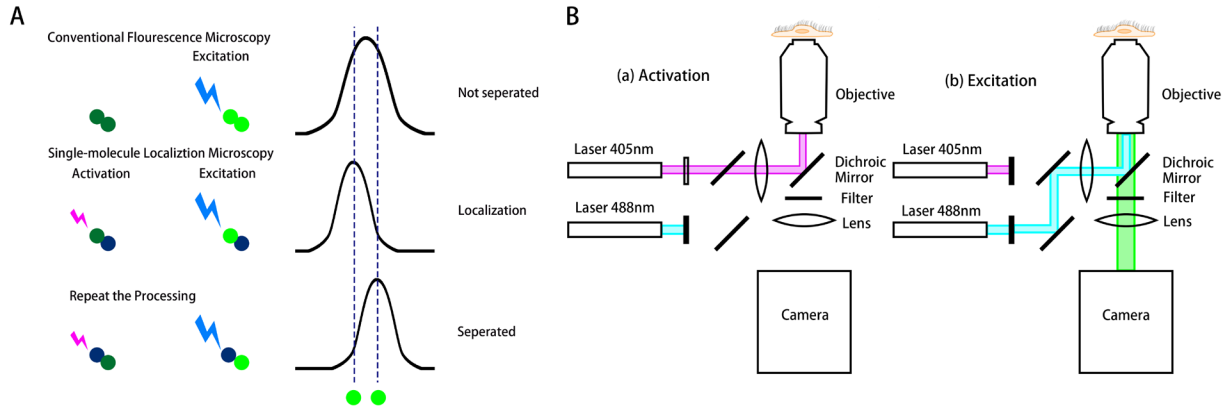

Figure 1. Schematics of the working principle and the setup of the stochastic optical reconstruction microscopy (STORM). (**A**) The top row shows the two fluorophores (located along the two dashed lines) activated and excited simultaneously by conventional microscopy. Due to the diffraction limit, the two fluorophores cannot be separated, resulting in a blurring image. The middle and bottom rows show the principle of STORM for the localization of a single molecule to a nanometer accuracy. The fluorophores are activated and excited not simultaneously, but sequentially to be localized and separated with each other. This technique can overcome the diffraction barrier for the conventional fluorescence microscopy. (**B**) A representative optical set up of STORM for the fluorophore Auto 488. (a) The optical path in activation process. The 405nm wavelength laser activates the photo-switchable fluorophore Auto 488, enabling the excitation. (b) The optical path in excitation and imaging processes. The 488nm laser excites the activated "on" fluorophore and its emission is recorded by a camera.

have a higher image collection efficiency, however, the distance between adjacent emitters must be greater than their PSF to distinguish each other for conventional microscopy. To trade the super spatial resolution (accuracy), STORM sacrifices its temporal resolution (efficiency) by switching the state and sequentially exciting the emitters at high density. Rust *et al*. [7] employed organic dyes and fluorescent proteins as photo-switchable emitters to trade temporal resolution for a super spatial resolution (~20 nm lateral and ~50 nm axial at present, can go down to a couple of nanometers if using smaller peptides or anti-body fragments instead of currently used whole anti-bodies), which is an order of magnitude higher than conventional confocal microscopy. STORM can perform 2D [7], 3D [12], and multicolor [13] imaging. In each frame of a STORM movie, a set of emitters is randomly activated so that locations of single emitters isolated within their PSFs can be spatially resolved.

Since it was developed, STORM has been employed in many biomedical researches. A number of subcellular structures including microtubules, actin, clathrin-coated pits, mitochondria, endoplasmic reticulum, and focal adhesion complexes have been visualized by STORM [11], as well as protein organization in bacteria [19] and molecular architecture of nerve synapses [20]. Using STORM with data processed by the affiliated algorithm, the super resolution images of ESG components at the surface of cultured EC monolayers were first revealed with unprecedented spatio-chemical resolution [21,22] and will be described in more details below.

ENDOTHELIAL SURFACE GLYCOCALYX: COMPOSITION, STRUCTURE, AND FUNCTION

Vascular ECs line the inner wall of every blood vessel. In addition to forming a transport barrier between the blood and vessel wall, vascular ECs play important roles in regulating circulation functions. Besides biochemical stimuli, blood flow induced (hemodynamic) mechanical stimuli, modulate EC morphology and functions by activating mechanosensors, signaling pathways, and gene and protein expressions [23]. EC responses to the hemodynamic forces (mechano-sensing and transduction) are critical to maintaining normal vascular functions [24,25]. Failure in mechano-sensing and transduction contributes to serious vascular diseases including hypertension, atherosclerosis, aneurysms, stroke, thrombosis, and cancer, to name a few [4,26-28].

Function

The functions of vascular ECs are determined by their structural components. The luminal surface of the ECs is coated with a glycocalyx of membrane-bound macromolecules comprised of sulfated proteoglycans and GAGs, glycoproteins and plasma proteins that adhere to this surface matrix. Due to its unique location, at the in-

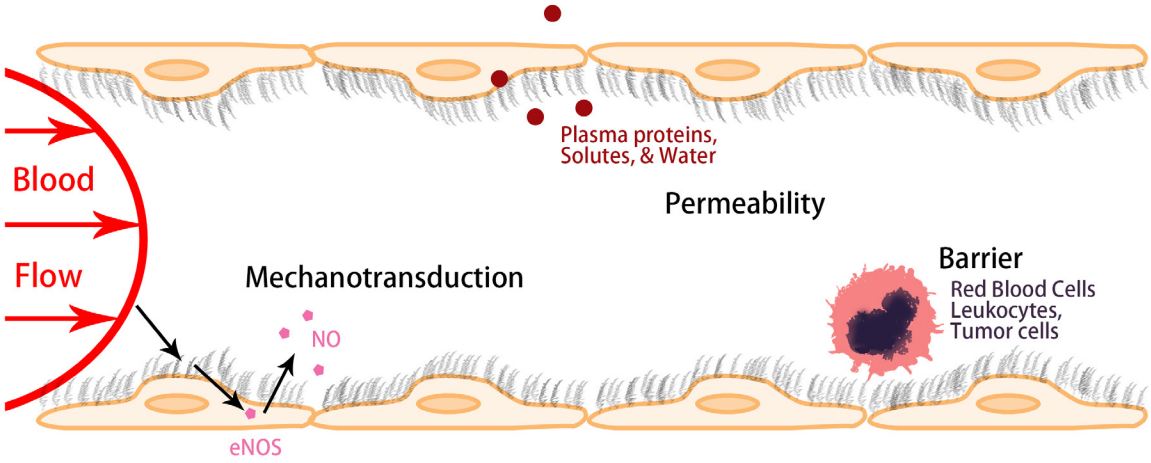

Figure 2. Schematic showing the major roles of the endothelial surface glycocalyx (ESG) in regulating vascular functions. As a mechanosensor and transducer to the blood flow, as a molecular sieve to main the normal vascular permeability and as a barrier to circulating cells including red blood cells, leukocytes, and tumor cells.

terface of circulating blood and vascular ECs, ESG plays important roles in maintaining vascular functions. Figure 2 summarizes three major roles of ESG: 1) It can serve as a mechanosensor and transducer for the ECs to sense the blood flow; 2) It maintains normal microvessel permeability by forming a molecular sieve, which allows the passage of water and small molecules but restricts large molecules such as plasma proteins; and 3) It generates a lubrication buffer between circulating red blood cells (RBCs) and ECs forming the vessel wall to avoid RBCs damage, and a barrier to prevent adhesion of circulating leukocytes, platelets, and tumor cells to the vessel wall [4]. It also shields EC surface receptors, preventing their hyperactivation [22].

Molecular Composition and Organization

The roles of ESG are based on its molecular composition and organization [3,4,29]. The components of the ESG have been investigated in depth [28,30]. The ESG is mainly composed of glycoproteins bearing short acidic oligosaccharides and terminal SAs, and PGs like heparan sulfate PGs (HSPG) including syndecan and glypican core proteins with long GAG side chains. The negatively charged GAGs bind proteins, growth factors, cations, and other plasma components. The predominant GAGs in vascular ECs are HS, CS, and HA. Of the three, the most abundant is HS, accounting for 50 to 90 percent of the total GAGs, the rest being comprised of CS and HA [31]. HS and CS are covalently bound to PGs, whereas HA does not bind to a PG core protein. HA is a non-sulfated GAG, which binds with its surface receptors CD44 and receptor for HA-mediated motility (RHAMM) [29].

It is widely believed that the negatively charged GAGs in the ESG capture circulating plasma proteins and cations and form an interconnected gel-like structure in an aqueous environment [32-34], and that the ESG would collapse if a GAG component was significantly reduced. However, a recent study by Zeng *et al*. [30] observed that specific enzymatic removal of HS or HA did not result in cleavage or collapse of any of the remaining components. Simultaneous removal of CS and HA by chondroitinase did not affect HS. Their results suggest that all GAGs and adsorbed proteins are well inter-mixed within the structure of the ESG, but the GAG components do not interact with one another.

Thickness and Structure

In addition to its biochemical composition, the thickness and ultrastructure of the ESG determine its functions. The first visualization of the ESG by EM used the cationic dye ruthenium red that binds to acidic mucopolysaccharides and generates electron density in the presence of osmium tetroxide [35]. Subsequent studies [36,37] used gold colloids and immunoperoxidase labeling. Adamson and Clough [38] then demonstrated using a large charged marker protein (unable to penetrate the ESG), cationized ferritin (molecular weight ~450 kDa), that in the absence of plasma proteins, the ESG would collapse, presumably due to elimination of intramolecular interactions with plasma proteins, and that its undisturbed thickness was several times greater than the 20 nm observed with ruthenium red [35]. All of these methods may suffer from dehydration artifacts associated with aqueous fixatives that likely dissolve all but the protein cores of proteoglycans

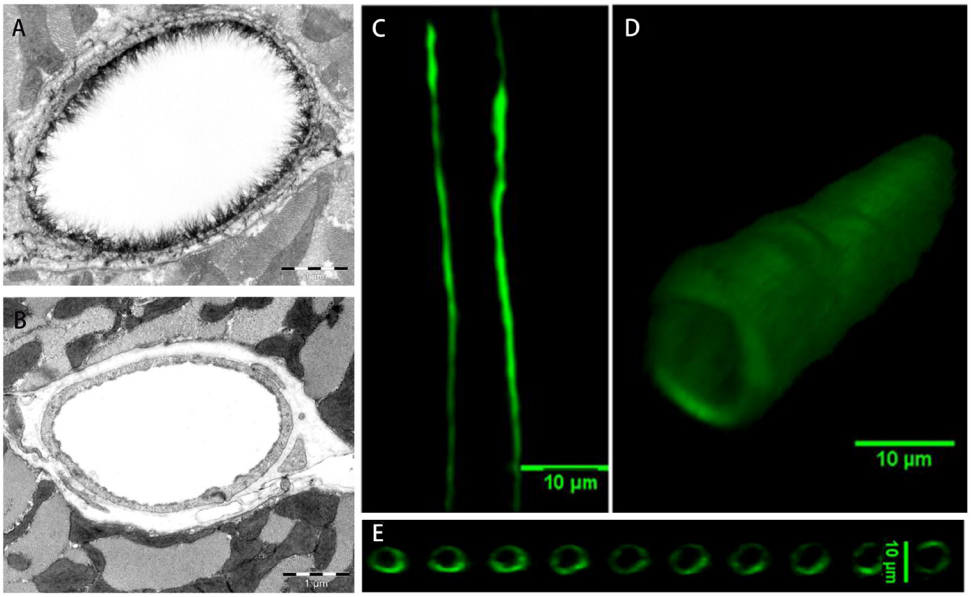

Figure 3. Visualization of the ESG by electron microscopy and confocal microscopy. Electron microscopic views of the ESG at a rat left ventricular myocardial capillary under control (A) and after enzymatic removal (B) [40]. Confocal microscopic views of the fluorescence conjugated anti-heparan sulfate (HS)-labeled ESG at a rat mesenteric capillary, mid-plane view (C), 3-D view (D) and the cross-sectional views along the vessel longitudinal direction (E) [49].

and collapse the inherently hydrated structures. A method developed to preserve water soluble structures using fluorocarbons as non-aqueous carriers of osmium tetroxide was applied to microvessels to obviate some of these limitations by Sims and Horne [37]. Further elaborations of the fluorocarbon-glutaraldehyde fixation methods by Rostgaard and Qvortrup [39] revealed a filamentous brush-like surface coating on capillary walls, but a layer thickness of less than 50 nm, suggesting a cleavage of more superficial matrix structures. All of the foregoing EM studies revealed an ESG with a thickness less than 100 nm. Recently, van den Berg *et al*. [40] used a new approach to stabilize the anionic carbohydrate structures on the ESG by Alcian blue 8GX (Figure 3A, B). They found that the ESG thickness was 0.2-0.5 µm on rat left ventricular myocardial capillaries.

To overcome the artifact by EM, the amount of ESG was estimated based on the biophysical principles from *in vivo* observations [41]. A direct *in vivo* measurement of the ESG thickness with the dye-exclusion technique was developed by Vink and Duling [42]. Using a 70 kD FITC-dextran plasma tracer, which they showed was sterically excluded by the ESG, they were able to provide the first estimate of the *in vivo* thickness of the ESG in capillaries of hamster cremaster-muscle to be ~0.4-0.5 µm. Most recently, the ESG thickness was also estimated as ~0.5 µm in rat mesenteric post-capillary venules by FITC-dextran labeling with intravital microscopy [43]. This estimate of the *in vivo* thickness of the ESG is four to five times greater than previous estimates derived from EM studies. This discrepancy was a catalyst for much of the work that has followed on the estimation of ESG thickness and its function as a barrier in cellular interactions as well as a mechno-sensor and transducer of ECs.

The poor spatial resolution of an intravital optical microscope limits the accurate measurement of the ESG thickness [44]. New imaging methods have thus been developed by employing laser scanning confocal microscopy and multi-photon microscopy, and fluorescently tagged antibodies to HS or HA binding protein, or wheat germ agglutinin (WGA) to label major components of the ESG. Application of these new methods has revealed a much thicker ESG in large blood vessels: 4.3-4.5 µm in the mouse common carotid artery [45], 2.2 µm in the mouse internal carotid artery [46], and 2.5 µm in the external carotid artery [47]. Ebong *et al*. [48] presented the first cryo-EM images of *in vitro* ESG that avoided the dehydration artifacts of conventional EM and observed structures greater than 5 µm in thickness (up to ~11 µm). Most recently, using high sensitivity and resolution confocal microscopy and *in situ*/*in vivo* single microvessel and *ex vivo* aorta immunostaining, Yen *et al*. [49] revealed that the thickness of the ESG on rat mesenteric and mouse cremaster capillaries and post-capillary venules is 1-1.5 µm (Figure 3C, D, E). The ESG thickness is 2-2.5 µm on rat and mouse aorta. They also observed that the

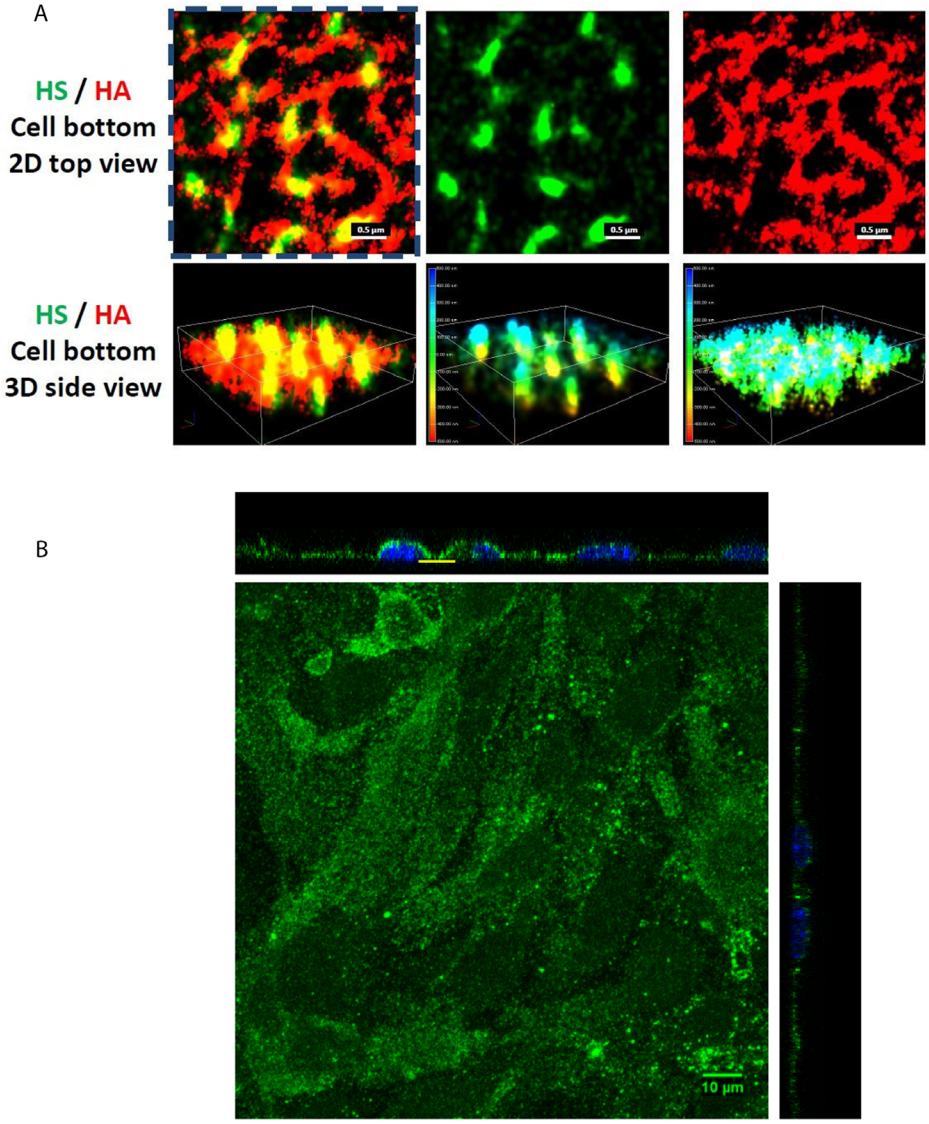

Figure 4. ESG components and ultrastructure visualized by STORM and by confocal microscopy (**A**) STORM images of the anti-heparan sulfate (HS) (green, middle panel) and anti-hyaluronic acid (HA) (red, right panel) of the ESG focusing at the bottom of a bEnd3 cell. The left panel is the overlay [21]. The color bars in the middle and right panels at the bottom row (3D side views) are the scale bars in nanometer. (**B**) Confocal images of the same anti-HS labeled ESG of the bEnd3 cells (mouse brain microvascular endothelial cell) [55]. Yellow line indicates the region for the STORM images.

ESG is continuously and evenly distributed on the aorta wall but not on the microvessel wall if looking at a vessel segment of length ~100 μm. By comparing the distance between the plasma membrane labeling and the labeling of ESG (SA residues) by WGA in a single microvessel *in vivo*, Betteridge *et al*. [50] found that the ESG thickness is 0.17-3.02 μm in the same type of microvessels as in Yen *et al.* [49], depending on the labeling and analyzing methods. However, the thickness of ESG at the same portion of the vessel is only ~0.08 μm observed by the EM through Alcian Blue labeling.

The ultrastructural organization of the ESG and its relation to the cytoskeleton components (*e.g.*, F-actin) of ECs was first investigated by Squire *et al*. [51] Using computed autocorrelation functions and Fourier transforms of EM images of frog mesenteric microvessels, they estimated a quasi-periodic substructure in the ESG, which is a 3D fibrous meshwork with characteristic

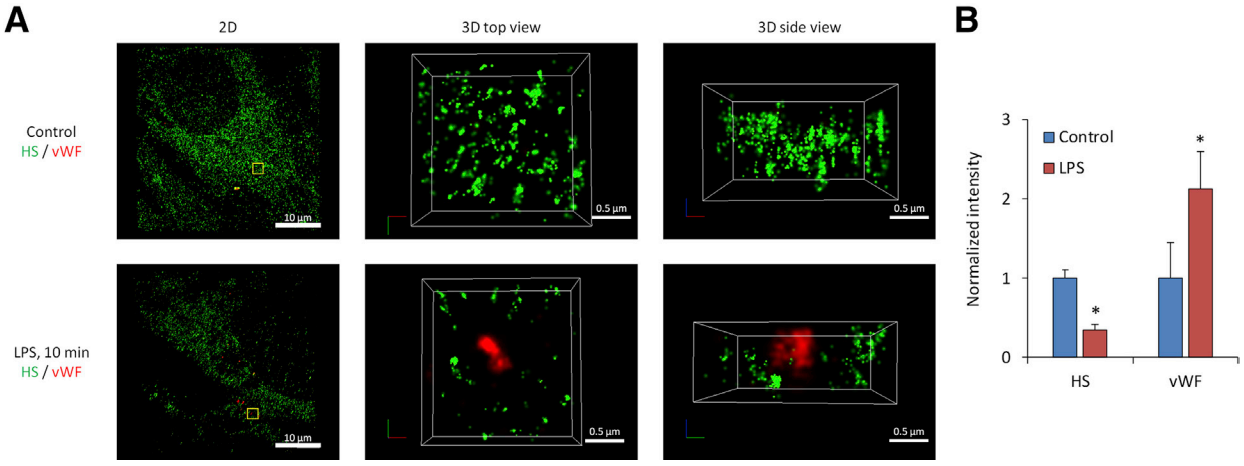

Figure 5. Visualization of the ESG and vWF labeled-WPB by STORM. The anti-HS labeled ESG (green) and anti-vWF (red) labeled-WPB images acquired by STORM for a bEnd3 cell. The top row in (**A**) shows those under control and the bottom row shows those after 10 min lipopolysaccharides (LPS) treatment. The left panel is the 2-D overview of a 40μm×40μm image focusing at the bottom of an endothelial cell. An enlarged top view of a yellow box (approximately 2μm × 2μm) in the left panel is shown in the middle panel and its side view in the right panel. (**B**) Relative intensity of the anti-HS and anti-vWF-labeled WPBs after 10 min LPS treatment compared to the control. vWF, von Willebrand factor; WPB, Weibel-Palade body [22].

spacing ~20 nm. The recent study by Arkill *et al*. [52] observed similar ESG structures in mammalian microvessels of choroid, renal tubules, glomerulus, and psoas muscle, and was confirmed by a 3D reconstruction using electron tomography by employing a tannic acid staining method and a novel staining technique of Lanthanum Dysprosium Glycosamino Glycan adhesion (the LaDyGAGa method) [53]. The thickness of the ESG observed by their EM method is ~100 nm, similar to what was previously found on frog mesenteric microvessels [38]. Based on these studies, the approximately 100 nm thick structure may form an inner core of the ESG which might determine the filtration and molecular sieve function of the microvessel wall to water and solutes while a micron scale outer structure might generate a buffer region for the lubrication of RBC movement and a barrier for leukocyte and tumor cell adhesion to the ECs forming the vessel wall. But how this structure plays a role in mechano-sensing and transduction remains to be elucidated.

COMPONENTS AND ULTRASTRUCTURE OF THE ESG REVEALED BY STORM

The recent development of ultra-resolution STORM has made it possible to visualize the spatio-chemical organization of the intact ESG at high resolution [22,54]. STORM employs organic dyes and fluorescent proteins as photo-switchable emitters to trade temporal resolution for a super spatial resolution (20 nm lateral and 50 nm axial at present due to the size of antibodies used to identify the ESG components), which is an order of magnitude greater than conventional confocal microscopy [7].

Spatio-Chemical Organization of Intact ESG

The spatio-chemical organization of the intact ESG at EC (bEnd3, mouse brain microvascular endothelial cell) monolayers was first observed by using Nikon-STORM [21]. After confluent, the bEnd3 cells were immunolabeled with anti-HS, followed by an ATTO488 conjugated goat anti-mouse IgG, and with biotinylated HA binding protein, followed by an AF647 conjugated anti-biotin. The ESG was then imaged by the STORM with a 100×/1.49 oil immersed lens. Multiple Reporters of ATTO488 and AF647 with alternating illumination were used to acquire the 3D images of HS and HA. The field of 256 × 256 (40 × 40 μm^2) of HS and HA at the surface of ECs was obtained based on total 40,000 of EM-CCD captured images for each reporter at a capturing speed of 19 ms/frame. Figure 4A demonstrates the STORM images for the HA (top view, red, top row on the right) and HS (green, top row in the middle) and overlay (top row on the left) of the ESG focused at the bottom surface of the bEnd3 cells (yellow line indicated region in Figure 4B). Figure 4B is a confocal microscopic view of the same ESG of bEnd3 cells labeled with anti-HS [55]. The EC plasma membrane is located at the bottom plane of the 3D images (bottom row). The color bars in the 3D side views are the scale bars in nanometer. The

figure shows that HA is a long molecule weaving into a network, which is horizontal to the EC cell surface. In contrast, HS is a shorter molecule, which is perpendicular to the cell surface. The height of the HS is ~800 nm. HA and HS seem to overlap with each other at the EC surface. The revealed ultrastructure of ESG by STORM suggests that HS plays a major role in mechanosensing and HA plays a major role in forming the molecular sieve.

Damage of ESG Observed by STORM at the Onset of Sepsis

Damage to and modification of the ESG have been observed in many diseases including diabetes, ischemia, myocardial edema, chronic infectious diseases, atherosclerosis, and tumor metastasis [27,28,40,56-62,63]. Sepsis is a systemic inflammatory syndrome induced by bacterial infection that can lead to multiorgan failure. Recently, Zullo *et al.* [22] employed the STORM to investigate the molecular mechanism by which lipopolysaccharide (LPS, an endotoxin secreted by bacteria during sepsis) induces a patchy loss of ESG at the onset of sepsis. They found that the loss of ESG is the result of exocytosis of endothelial lysosome- related organelles including Weibel-Palade bodies (WPB) and secretory lysosomes. Figure 5 demonstrates that under control (Figure 5A, top row), ESG was richly presented by fluorescently labeled anti-HS antibodies. However, after 10 min LPS treatment, von Willebrand factor (vWF)-labeled WPB became externalized and was surrounded by the halo areas of lost HS-decorated ESG (Figure 5A, bottom row). Only the super-resolution STORM could make it possible to observe such a nano-scaled picture for the ESG and exocytotic vWF/WPBs. Figure 5B shows the relative intensity of anti-HS and vWF/WPBs after LPS treatment compared with the control.

CONCLUSION

Although the ESG has been studied for over a half-century since the 1960s for its composition, structure and function, its detailed components and ultrastructure in its native cellular environment have just started to be investigated owing to the recent development of super-resolution optical microscopy such as STORM. Due to its heterogeneous structures, complex composition of various proteoglycans, GAGs, and absorbed plasma proteins, attachment to the transmembrane glycoproteins and receptors, as well as EC cytoskeleton and plasma membrane, its functions as a mechanosensor, a barrier to the interaction between circulating cells to ECs lining the vascular wall and a molecular sieve to water and solutes are expected to be governed by multiple mechanisms. By employing STORM, we can first elucidate its various components and their organization under physiological conditions and explore the molecular and cellular mechanisms by which these structures and organizations are modulated under pathological conditions.

Since the spatial resolution of the STORM is determined not only by the optical parts of the microscope, but largely by the suitable photo-switchable probes, *i.e.*, the half-life of the fluorophore as well as the size of the specific biomarker such as antibodies used in the current studies. In the future studies for the ESG, we will further improve the resolution by finding longer half-life fluorophores and smaller biomarkers such as small peptides and fragments of antibodies. The STORM resolution is also limited by how fast a computer can acquire and analyze the images. In addition to updating high performance computers, we will create more efficient computational algorithms. The resolution can also be improved by post-image processing techniques.

Acknowledgments: This work is supported in part by NIH RO1NS101362-01 and 1UG3TR002151-01. We thank Ms. Boen Yin for her helps in diagram drawing.

REFERENCES

1. Abbe E. Beiträge zur Theorie des Mikroskops und der mikroskopischen Wahrnehmung. Archiv für mikroskopische Anatomie. 1873;9(1):413-8.
2. Tarbell JM, Ebong EE. The endothelial glycocalyx: a mechano-sensor and-transducer [-pt.]. Sci Signal. 2008;1(40):pt8.
3. Tarbell JM, Pahakis MY. Mechanotransduction and the glycocalyx. J Intern Med. 2006;259(4):339–50.
4. Fu BM, Tarbell JM. Mechano-sensing and transduction by endothelial surface glycocalyx: composition, structure, and function. Wiley Interdiscip Rev Syst Biol Med. 2013;5(3):381–90.
5. Hell SW, Wichmann J. Breaking the diffraction resolution limit by stimulated emission: stimulated-emission-depletion fluorescence microscopy. Opt Lett. 1994;19(11):780–2.
6. Moerner WE. New directions in single-molecule imaging and analysis. Proc Natl Acad Sci USA. 2007;104(31):12596–602.
7. Rust MJ, Bates M, Zhuang X. Sub-diffraction-limit imaging by stochastic optical reconstruction microscopy (STORM). Nat Methods. 2006;3(10):793–5.
8. Betzig E, Patterson GH, Sougrat R, Lindwasser OW, Olenych S, Bonifacino JS, et al. Imaging intracellular fluorescent proteins at nanometer resolution. Science. 2006;313(5793):1642–5.
9. Hess ST, Girirajan TP, Mason MD. Ultra-high resolution imaging by fluorescence photoactivation localization microscopy. Biophys J. 2006;91(11):4258–72.
10. Xie XS, Choi PJ, Li GW, Lee NK, Lia G. Single-molecule approach to molecular biology in living bacterial cells. Annu Rev Biophys. 2008;37:417–44.
11. Huang B, Babcock H, Zhuang X. Breaking the diffraction barrier: super-resolution imaging of cells. Cell.

2010;143(7):1047–58.
12. Huang B, Wang W, Bates M, Zhuang X. Three-dimensional super-resolution imaging by stochastic optical reconstruction microscopy. Science. 2008;319(5864):810–3.
13. Bates M, Huang B, Dempsey GT, Zhuang X. Multicolor super-resolution imaging with photo-switchable fluorescent probes. Science. 2007;317(5845):1749–53.
14. Sydor AM, Czymmek KJ, Puchner EM, Mennella V. Super-Resolution Microscopy: From Single Molecules to Supramolecular Assemblies. Trends Cell Biol. 2015;25(12):730–48.
15. Patterson G, Davidson M, Manley S, Lippincott-Schwartz J. Superresolution imaging using single-molecule localization. Annu Rev Phys Chem. 2010;61:345–67.
16. Jones SA, Shim SH, He J, Zhuang X. Fast, three-dimensional super-resolution imaging of live cells. Nat Methods. 2011;8(6):499–508.
17. Baddeley D, Bewersdorf J. Biological Insight from Super-Resolution Microscopy: What We Can Learn from Localization-Based Images. Annu Rev Biochem. 2018;87(1).
18. Hell SW. Far-field optical nanoscopy. Science. 2007;316(5828):1153-8.
19. Greenfield D, McEvoy AL, Shroff H, Crooks GE, Wingreen NS, Betzig E, et al. Self- organization of the Escherichia coli chemotaxis network imaged with super-resolution light microscopy. PLoS Biol. 2009;7(6):e1000137.
20. Dani A, Huang B, Bergan J, Dulac C, Zhuang X. Superresolution imaging of chemical synapses in the brain. Neuron. 2010;68(5):843–56.
21. Fan J, Sun Y. John Tabell, Bingmei Fu. Ultra-Structure of Endothelial Surface Glycocalyx Revealed by Stochastic Optical Reconstruction Microscopy (STORM) [San Diego.]. FASEB J. 2018;EB2018(April):21–5.
22. Zullo JA, Fan J, Azar TT, Yen W, Zeng M, Chen J, et al. Exocytosis of Endothelial Lysosome-Related Organelles Hair-Triggers a Patchy Loss of Glycocalyx at the Onset of Sepsis. Am J Pathol. 2016;186(2):248–58.
23. Mammoto A, Mammoto T, Ingber DE. Mechanosensitive mechanisms in transcriptional regulation. J Cell Sci. 2012;125(Pt 13):3061–73.
24. Davies PF, Dewey CF, Bussolari SR, Gordon EJ, Gimbrone M. Influence of hemodynamic forces on vascular endothelial function. In vitro studies of shear stress and pinocytosis in bovine aortic cells. J Clin Invest. 1984;73(4):1121–9.
25. Chien S. Mechanotransduction and endothelial cell homeostasis: the wisdom of the cell. Am J Physiol Heart Circ Physiol. 2007;292(3):H1209–24.
26. Ingber D. Mechanobiology and diseases of mechanotransduction. Ann Med. 2009;35(8):564–77.
27. Cai B, Fan J, Zeng M, Zhang L, Fu BM. Adhesion of malignant mammary tumor cells MDA-MB-231 to microvessel wall increases microvascular permeability via degradation of endothelial surface glycocalyx. J Appl Physiol (1985). 2012;113(7):1141-53.
28. Tarbell JM, Cancel LM. The glycocalyx and its significance in human medicine. J Intern Med. 2016;280(1):97–113.
29. Zeng Y. Endothelial glycocalyx as a critical signalling platform integrating the extracellular haemodynamic forces and chemical signalling. J Cell Mol Med. 2017;21(8):1457–62.
30. Zeng Y, Ebong EE, Fu BM, Tarbell JM. The structural stability of the endothelial glycocalyx after enzymatic removal of glycosaminoglycans. PLoS One. 2012;7(8):e43168.
31. Sarrazin S, Lamanna WC, Esko JD. Heparan sulfate proteoglycans. Cold Spring Harb Perspect Biol. 2011;3(7).
32. Ohlson M, Sorensson J, Haraldsson B. A gel-membrane model of glomerular charge and size selectivity in series. Am J Physiol Renal Physiol. 2001;280(3):F396–405.
33. Sörensson J, Ohlson M, Haraldsson B. A quantitative analysis of the glomerular charge barrier in the rat. Am J Physiol Renal Physiol. 2001;280(4):F646–56.
34. Weinbaum S, Tarbell JM, Damiano ER. The structure and function of the endothelial glycocalyx layer. Annu Rev Biomed Eng. 2007;9:121–67.
35. Luft JH, editor. Fine structures of capillary and endocapillary layer as revealed by ruthenium red. Federation proceedings; 1966.
36. Baldwin A, Winlove C. Effects of perfusate composition on binding of ruthenium red and gold colloid to glycocalyx of rabbit aortic endothelium. J Histochem Cytochem. 1984;32(3):259–66.
37. Sims DE, Horne MM. Non-aqueous fixative preserves macromolecules on the endothelial cell surface: an in situ study. Eur J Morphol. 1994;32(1):59–64.
38. Adamson R, Clough G. Plasma proteins modify the endothelial cell glycocalyx of frog mesenteric microvessels. J Physiol. 1992;445(1):473–86.
39. Rostgaard J, Qvortrup K. Electron microscopic demonstrations of filamentous molecular sieve plugs in capillary fenestrae. Microvasc Res. 1997;53(1):1–13.
40. van den Berg BM, Vink H, Spaan JA. The endothelial glycocalyx protects against myocardial edema. Circ Res. 2003;92(6):592–4.
41. Klitzman B, Duling BR. Microvascular hematocrit and red cell flow in resting and contracting striated muscle. Am J Physiol Heart Circ Physiol. 1979;237(4):H481–90.
42. Vink H, Duling BR. Identification of distinct luminal domains for macromolecules, erythrocytes, and leukocytes within mammalian capillaries. Circ Res. 1996;79(3):581–9.
43. Long DS, Smith ML, Pries AR, Ley K, Damiano ER. Microviscometry reveals reduced blood viscosity and altered shear rate and shear stress profiles in microvessels after hemodilution. Proc Natl Acad Sci USA. 2004;101(27):10060–5.
44. Pries A, Secomb T, Gaehtgens P. The endothelial surface layer. Pflugers Arch. 2000;440(5):653–66.
45. van den Berg BM, Spaan JA, Vink H. Impaired glycocalyx barrier properties contribute to enhanced intimal low-density lipoprotein accumulation at the carotid artery bifurcation in mice. Pflugers Arch. 2009;457(6):1199–206.
46. Reitsma S, oude Egbrink MG, Vink H, Van Den Berg BM, Passos VL, Engels W, et al. Endothelial glycocalyx structure in the intact carotid artery: a two-photon laser scanning microscopy study. J Vasc Res. 2011;48(4):297–306.
47. Megens R, Reitsma S, Schiffers P, Hilgers R, De Mey J, Slaaf D, et al. Two-photon microscopy of vital murine elastic and muscular arteries. J Vasc Res. 2007;44(2):87–98.
48. Ebong EE, Macaluso FP, Spray DC, Tarbell JM. Imaging

the endothelial glycocalyx in vitro by rapid freezing/freeze substitution transmission electron microscopy. Arterioscler Thromb Vasc Biol. 2011;31(8):1908–15.
49. Yen WY, Cai B, Zeng M, Tarbell JM, Fu BM. Quantification of the endothelial surface glycocalyx on rat and mouse blood vessels. Microvasc Res. 2012;83(3):337–46.
50. Betteridge K, Arkill K, Neal C, Harper S, Foster B, Satchell S, et al. Sialic acids regulate microvessel permeability, revealed by novel in vivo studies of endothelial glycocalyx structure and function. J Physiol. 2017.
51. Squire S. A chance to grow. Professional nurse (London, England). 2001;16(8 Suppl):S2-S.
52. Arkill K, Knupp C, Michel C, Neal C, Qvortrup K, Rostgaard J, et al. Similar endothelial glycocalyx structures in microvessels from a range of mammalian tissues: evidence for a common filtering mechanism? Biophys J. 2011;101(5):1046–56.
53. Arkill KP, Neal CR, Mantell JM, Michel CC, Qvortrup K, ROSTGAARD J, et al. 3D reconstruction of the glycocalyx structure in mammalian capillaries using electron tomography. Microcirculation. 2012;19(4):343–51.
54. Song JW, Zullo J, Lipphardt M, Dragovich M, Zhang FX, Fu B, et al. Endothelial glycocalyx—the battleground for complications of sepsis and kidney injury. Nephrol Dial Transplant. 2017.
55. Fan J, Fu BM. Quantification of malignant breast cancer cell MDA-MB-231 transmigration across brain and lung microvascular endothelium. Ann Biomed Eng. 2016;44(7):2189–201.
56. Reitsma S, Slaaf DW, Vink H, Van Zandvoort MA, Oude Egbrink MG. The endothelial glycocalyx: composition, functions, and visualization. Pflugers Arch. 2007;454(3):345–59.
57. Becker BF, Chappell D, Bruegger D, Annecke T, Jacob M. Therapeutic strategies targeting the endothelial glycocalyx: acute deficits, but great potential. Cardiovasc Res. 2010;87(2):300–10.
58. Chappell D, Heindl B, Jacob M, Annecke T, Chen C, Rehm M, et al. Sevoflurane reduces leukocyte and platelet adhesion after ischemia-reperfusion by protecting the endothelial glycocalyx. Anesthesiology. 2011;115(3):483–91.
59. Schmidt EP, Yang Y, Janssen WJ, Gandjeva A, Perez MJ, Barthel L, et al. The pulmonary endothelial glycocalyx regulates neutrophil adhesion and lung injury during experimental sepsis. Nat Med. 2012;18(8):1217.
60. Becker BF, Jacob M, Leipert S, Salmon AH, Chappell D. Degradation of the endothelial glycocalyx in clinical settings: searching for the sheddases. Br J Clin Pharmacol. 2015;80(3):389–402.
61. Marki A, Esko JD, Pries AR, Ley K. Role of the endothelial surface layer in neutrophil recruitment. J Leukoc Biol. 2015;98(4):503–15.
62. Potter DR, Van Teeffelen J, Vink H, van den Berg BM. Perturbed mechanotransduction by endothelial surface glycocalyx modification greatly impairs the arteriogenic process. American Journal of Physiology-Heart and Circulatory Physiology. 2015;309(4):H711-H7.
63. Rai S, Nejadhamzeeigilani Z, Gutowski NJ, Whatmore JL. Loss of the endothelial glycocalyx is associated with increased E-selectin mediated adhesion of lung tumour cells to the brain microvascular endothelium. J Exp Clin Cancer Res. 2015;34(1):105.